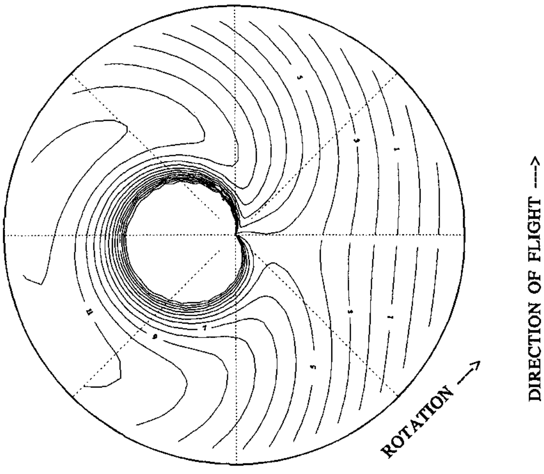

Fig. 4 Blade angle of attack with optimized second order harmonic input. Speed 140 kt, power consumption 3251 hp.

lows: at a given airspeed, vary ϕ_2 to minimize the power. With that value of ϕ_2, vary a_2 to minimize the power. With both a_2 and ϕ_2 determined, increase the speed. Eventually, a speed is reached when flight can no longer be sustained with the current a_2 and ϕ_2. This is signaled by the blade state and rotor loads failing to converge. Backing off, to a speed where convergence occurs ϕ_2, then a_2 are varied again to find the local optimum. With this done, further increase in speed is possible.

The procedure was repeated until a further increase of 1 kt was no longer possible. This speed (160 kt) is accepted as the top speed with second harmonic control. Note that the speed entry in each line in Table 1 above 150 kt is the top speed possible with a_2 and ϕ_2 of the previous line. The top speed with pure swashplate control was similarly determined and found to be 141 kt.

Figures 3 and 4 are contour plots of the blade angle of attack over the rotor disk. Both were taken at the same speed of 140 kt, Fig. 3 with pure swashplate control, Fig. 4 with optimum second harmonic control. These figures show how the use of $\kappa(\psi)$ shrinks the areas of high angle of attack experienced by the retreating blade.

V. Conclusions

The results given here generally corroborate the predictions of Ref. 3 regarding the increase in helicopter top speed with second harmonic control. However, the speed improvement is more modest than predicted there and the optimal control parameters that achieve it are not quite the same. (In our notation the control parameters in Ref. 3 are $a_2 = 4.1$ deg, $\phi_2 = -104$ deg, compare to the last line in Table 1.) The present work employs a full, nonlinear, dynamic model of the flapping blades, which offers a more solid basis for the analysis. More detailed results, such as the variation of optimal second harmonic control with speed, fall out.

For continuity and comparison, we treated Arcidiacono's sample helicopter. This allows a direct comparison of the current blade simulation approach and its results to previous work. The actual increase in top speed is specific to the example treated. But the use of blade models such as Bladehelo is a general method whose time has come. Refining blade models and putting them to use for determining optimal methods of blade control opens a rich field of investigation.

Acknowledgment

The author wishes to thank his student Kenneth Graham for use of the blade computer model—Bladehelo—and for fruitful discussions.

References

[1]Stewart, W., "Second Harmonic Control on the Helicopter Rotor," Reports and Memoranda of the Aeronautical Research Council (Great Britain), Ministry of Supply, No. 2997, London, Aug. 1952.

[2]Payne, P. R., "Higher Harmonic Rotor Control," *Aircraft Engineering*, Vol. 30, No. 354, 1958, pp. 222–226.

[3]Arcidiacono, P. J., "Theoretical Performance of Helicopters Having Second and Higher Harmonic Feathering Control," *Journal of the American Helicopter Society*, Vol. 6, No. 1, 1961, pp. 8–19.

[4]Carlock, G. W., Garner, J. G., Guin, K. F., and Reyes, P. A., "Individual Blade Control," U.S. Patent 4,379,678, April 12, 1983.

[5]McArdle, F. H., "Helicopter Rotor Control System with Integrated Hub," U.S. Patent 4,534,704, Aug. 13, 1985.

[6]Ham, N. D., "Helicopter Individual Blade Control System," U.S. Patent 4,519,743, May 28, 1985.

[7]Wham, J. L., Mackey, L. A., and Haselton, F. R., "Propeller System with Electronically Controlled Cyclic and Collective Blade Pitch," U.S. Patent 4,648,345, March 10, 1987.

[8]Khan, Z. N., "Electro-Hydraulic Helicopter System Having Individual Blade Control," U.S. Patent 4,899,641, Feb. 13, 1990.

[9]Aubry, J. A., and Deguise, M., "Hydraulic Device for Individual Control of Pitch of a Rotor Blade," U.S. Patent 4,946,354, Aug. 7, 1990.

[10]Aubry, J. A., and Mondet, J. J., "Individual Pitch Control Device for Blades of Rotors of Rotor Craft by Means of Rotating Linear Jacks," U.S. Patent 5,011,373, April 30, 1991.

[11]Graham, K. S., and Katz, A., "A Blade Element Rotor Model in a Low Cost Helicopter Simulator," *Proceedings of the AIAA Simulation Technologies Conference* (Scottsdale, AZ), AIAA, Washington, DC, 1994, pp. 287–293 (AIAA Paper 94-3436).

[12]Graham, K. S., "Development of a Rotor Blade Model and Its Application to a Helicopter Simulator," M.S. Thesis, Univ. of Alabama, Tuscaloosa, AL, 1994.

Ice Accretion on Aircraft Wings with Thermodynamic Effects

P. Tran,* M. T. Brahimi,† and I. Paraschivoiu‡
École Polytechnique de Montréal,
Montreal, Quebec H3C 3A7, Canada
A. Pueyo§
University of Toronto,
Toronto, Ontario M5S 1A1, Canada
and
F. Tezok¶
Advanced Aerodynamics, Bombardier Inc./Canadair,
Dorval, Quebec H4S 1Y9, Canada

Nomenclature

C_D = drag coefficient
D = droplet diameter, m

Presented as Paper 94-0605 at the AIAA 32nd Aerospace Sciences Meeting and Exhibit, Reno, NV, Jan. 10–13, 1994; received Feb. 8, 1994; revision received June 1, 1994; accepted for publication June 1, 1994.

*Ph.D. Student, C.P. 6079, Succ. Centre Ville. Student Member AIAA.

†Research Associate, Department of Mechanical Engineering, C.P. 6079, Succ. Centre Ville. Student Member AIAA.

‡Bombardier Chair Professor, Department of Mechanical Engineering. Member AIAA.

§Ph.D. Student, Institute of Aerospace Studies. Student Member AIAA.

¶Advanced Aerodynamic Staff. Member AIAA.

$\dot{E}$ = internal energy rate, J/s
$\dot{H}$ = enthalpy rate, J/s
LWC = liquid water content, g/m^3
$\dot{m}$ = mass flow rate, kg/s
$\dot{Q}$ = heat flux rate, J/s
Re = Reynolds number
r_d = droplet position, m
T = temperature, °C
V = velocity vector, m/s
α = angle of attack, deg
μ = dynamic viscosity, kg/ms
ρ = density, kg/m^3

Subscripts
a = air
c = convection
d = droplet
f = friction
im = impingement
in = into control volume
ou = out of control volume
so = solidification
va = vaporization

Introduction

THE formation of ice on aircraft components such as wings, control surfaces, and engine intakes, occurs when the aircraft flies at a level where the temperature is at, or below freezing point and hits supercooled water droplets. The amount and the shape of ice collected depend mainly on liquid water content, temperature, airspeed, droplet size, and surface roughness. Results from wind-tunnel and flight icing tests indicate that the presence of ice on unprotected aircraft components can lead to a number of aerodynamic degradation problems, and consequently, is a major problem of safety.[1] The most severe penalties encountered deal with decreased maximum lift, increased drag, decreased stall angle, changes in the pressure distribution, early boundary-layer transition, increased stall speed, and reduced controllability. As a part of the research activities conducted by J.-A. Bombardier Aeronautical Chair at École Polytechnique de Montréal, numerical tools have been developed for ice accretion analysis and simulation that are of interest to Canadian aerospace industry[2,3] and are capable to predict the amount and shape of rime/glaze ice on aircraft including flowfield calculation, particle trajectory calculation, thermodynamic analysis and geometry update with the possibility of studying the effect of ambient temperature, roughness height, liquid water content, accretion time, droplet diameter, etc.

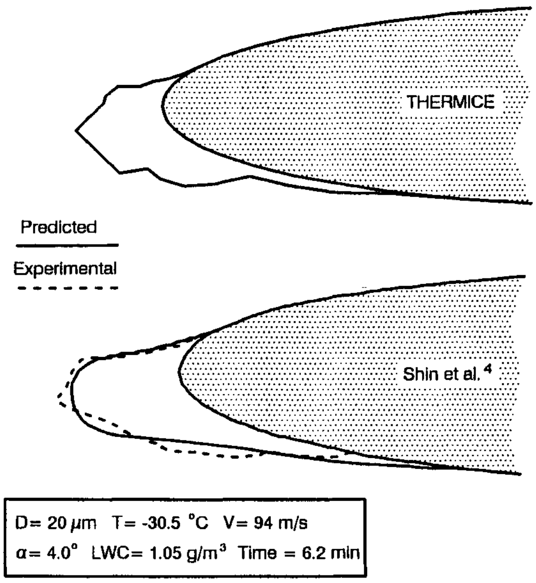

Fig. 1 Comparison of computed and experimental ice shapes in rime ice conditions ($T = -30.5$°C).

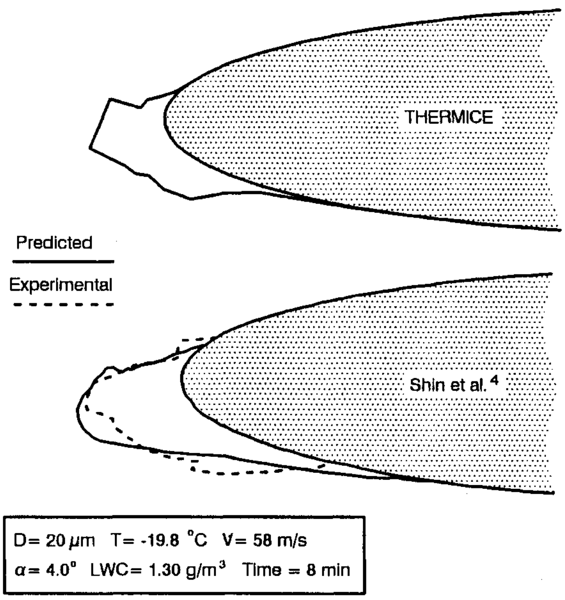

Fig. 2 Comparison of computed and experimental ice shapes in rime ice conditions ($T = -19.8$°C).

Simulation of Ice Accretion

The main objective of ice simulation is the calculation of the impingement of the particles on the wing, which determines the droplet impingement regions as well as the mass of liquid on the body surface. The main applications are for use as input to ice accretion calculation, to predict aerodynamic performance degradations, and for use in the design of anti/deicing systems. The computational procedure is an iterative process where the flowfield influences the ice formation which, in turn, changes the flowfield. At each integration step, the local velocity needed to solve the droplet equation of motion is obtained from the flowfield solution, while the integration is continued following droplets until they impinge on the airfoil surface or move out of the range of the limit trajectories. The present code is developed so that any panel code for flowfield computation could be matched with ice calculation modules. The procedure used for impact calculation is based on parametric equations for a droplet moving from one position to another. Then a condition on geometric parameters shows if a droplet does or does not hit the wing. The basic equation of motion for droplets, including the buoyancy, gravity and drag forces is

$$\frac{d^2\mathbf{r}_d}{dt^2} + \frac{C_D Re}{24}\frac{1}{K_A}\frac{d\mathbf{r}_d}{dt} = K_G + \frac{C_D Re}{24}\frac{1}{K_A}V_a \qquad (1)$$

with $K_G = [(\rho_d - \rho_a)/\rho_d]g$ and $K_A = \rho_d D_d^2/18\mu_a$. Equation (1) represents a second-order differential equation that can be solved using classical difference methods.

Thermodynamic Analysis

The thermodynamic characteristics of the freezing process of incoming droplets are analyzed by considering the mass and energy balance on the wing surface. Based on the mass flux and heat balance, the freezing fraction of the incoming water droplets for a control volume can be calculated, and along with the droplet impingement computation the amount and growth of ice formed on a control volume can be determined. The ambient temperature is critical in determining the type of surface involved: dry, wet, or liquid, and therefore,

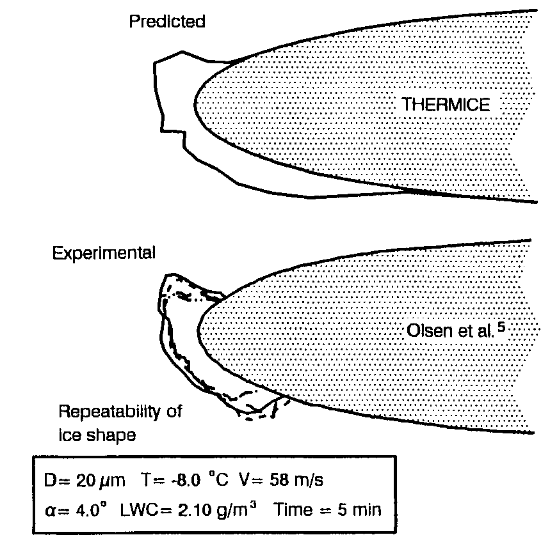

Fig. 3 Comparison of computed and experimental ice shapes in glaze ice conditions ($T = -8°C$).

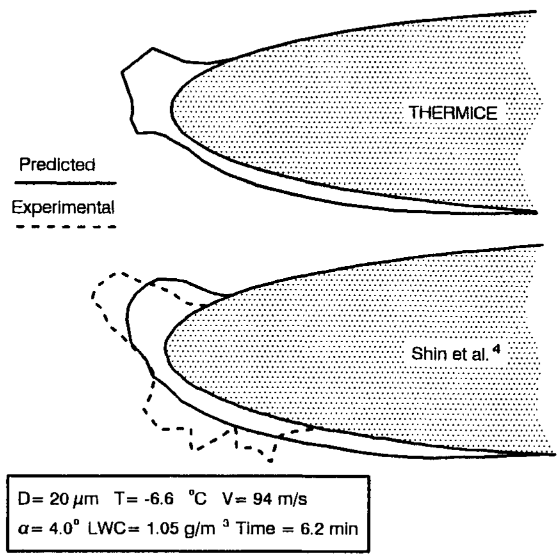

Fig. 4 Comparison of computed and experimental ice shapes in glaze ice conditions ($T = -6.6°C$).

on the energy balance. The continuity and energy equations are given by

$$\dot{m}_{\text{im}} + \dot{m}_{\text{in}} = \dot{m}_{\text{va}} + \dot{m}_{\text{ou}} + \dot{m}_{\text{so}} \tag{2}$$

$$\dot{E}_{\text{so}} + \dot{H}_{\text{va}} + \dot{H}_{\text{ou}} - \dot{H}_{\text{in}} - \dot{H}_{\text{im}} = \dot{Q}_f - \dot{Q}_c \tag{3}$$

Enthalpy and internal energy are calculated in relation to a given reference state and depend on the type of surface involved, whereas the heat transfer coefficient is computed from two relations, one for the laminar region and one for turbulent region.[3] The roughness model used is based on empirical relation as given by Ref. 4.

Results and Discussion

THERMICE has been tested in rime and glaze ice conditions and compared with experimental data and numerical results. Figures 1 and 2 show comparison between results calculated with THERMICE and those given by Shin et al.[4] in rime ice conditions. The calculated ice shape compares well with experimental data, particularly for the impingement limits on the upper and lower surface of the airfoil. Figure 3 shows comparison with a series of experiments conducted by Olsen et al.[5] in glaze ice conditions. We can observe that the horn is well-predicted, but the lower impingement limit, and consequently the accumulated mass of ice, is overestimated. Finally, Fig. 4 shows the resulting ice shape compared with experimental and numerical results at a temperature of −6.6°C. The results obtained with THERMICE compare well with the numerical data, but the experimental ice shape is not well-reproduced. This is the weakness of icing codes to predict glaze ice shape since there is limited understanding of the physical phenomenon of rough surfaces. Thus, it will be helpful if some experimental data could be obtained for heat transfer and roughness characterization.

Conclusions

An icing code including thermodynamic effects has been developed. It predicts well ice accretion in rime ice conditions. However, for glaze ice the results do not agree well with experimental data. For a realistic ice accretion it is important to include the microphysical aspect of ice, model accurately the convective heat transfer, and improve the correlations of equivalent sand-grain roughness.

Acknowledgment

The authors would like to acknowledge the support provided by Bombardier Inc./Canadair.

References

[1]Brumby, R. E., "Effects of Adverse Weather on Aerodynamics," *Proceedings of the Panel Specialists Meeting* (Toulouse, France), 1991, pp. 2.1–2.4 (AGARD CP 496).

[2]Mavriplis, F., "Icing and Contamination of Aircraft Surfaces: Industry's Concerns," *Proceedings of the First Bombardier International Workshop on Aircraft Icing and Boundary-Layer Stability and Transition*, edited by I. Paraschivoiu, Ecole Polytechnique de Montreal, Canada, 1993, pp. 51–55.

[3]Brahimi, M. T., Tran, P., and Paraschivoiu, I., "Numerical Simulation and Thermodynamic Analysis of Ice Accretion on Aircraft Wings," C.D.T., École Polytechnique de Montréal, Project C128, Canadair, Montreal, Canada, May 1994.

[4]Shin, J., Berkowitz, B., Chen, H., and Cebeci, T., "Prediction of Ice Shapes and Their Effect on Airfoil Drag," *Journal of Aircraft*, Vol. 31, No. 2, 1994, pp. 263–270.

[5]Olsen, W., Shaw, R., and Newton, J., "Ice Shapes and the Resulting Drag Increase for NACA 0012 Airfoil," NASA TM 83556, Jan. 1984.

Applicability of Newtonian and Linear Theory to Slender Hypersonic Bodies

Steven P. Kuester* and John D. Anderson Jr.†
University of Maryland,
College Park, Maryland 20742

Introduction

FOR many years, fluid dynamicists have looked for simple expressions to characterize aerodynamic properties for specific flow regimes. This has resulted in such expressions as the Prandtl-Glauert rule for subsonic lift coefficient ap-

Received April 11, 1994; revision received May 31, 1994; accepted for publication May 31, 1994.

*Graduate Research Assistant, Department of Aerospace Engineering, Bldg. 382. Student Member AIAA.

†Professor Aerospace Engineering, Department of Aerospace Engineering, Bldg. 88. Fellow AIAA.